Role of Hydrogen Bonding in the Active Site of Human Manganese Superoxide Dismutase † , ‡

ARTICLE *in* BIOCHEMISTRY · JULY 2004

Impact Factor: 3.02 · DOI: 10.1021/bi049888k · Source: PubMed

9 AUTHORS, INCLUDING:

Jeff Perry
University of California, Riverside
40 PUBLICATIONS **1,201** CITATIONS
SEE PROFILE

Diane E Cabelli
Brookhaven National Laboratory
91 PUBLICATIONS **3,150** CITATIONS
SEE PROFILE

M. Elizabeth Stroupe
Florida State University
34 PUBLICATIONS **485** CITATIONS
SEE PROFILE

John Tainer
University of Texas MD Anderson Cancer Center
458 PUBLICATIONS **30,197** CITATIONS
SEE PROFILE

Role of Hydrogen Bonding in the Active Site of Human Manganese Superoxide Dismutase[†,‡]

William B. Greenleaf,[§] J. Jefferson P. Perry,[∥] Amy S. Hearn,[§] Diane E. Cabelli,[⊥] James R. Lepock,[@] M. Elizabeth Stroupe,[∥] John A. Tainer,[∥] Harry S. Nick,[§] and David N. Silverman*[,§]

Departments of Pharmacology and Neuroscience, University of Florida, Gainesville, Florida 32610, Department of Molecular Biology, The Scripps Research Institute, La Jolla, California 92037, Chemistry Department, Brookhaven National Laboratory, Upton, New York 11973, and Department of Medical Biophysics, University of Toronto, Toronto, Ontario, Canada M5G 2M9

Received January 14, 2004; Revised Manuscript Received April 8, 2004

ABSTRACT: The side chain of Gln143, a conserved residue in manganese superoxide dismutase (MnSOD), forms a hydrogen bond with the manganese-bound solvent and is critical in maintaining catalytic activity. The side chains of Tyr34 and Trp123 form hydrogen bonds with the carboxamide of Gln143. We have replaced Tyr34 and Trp123 with Phe in single and double mutants of human MnSOD and measured their catalytic activity by stopped-flow spectrophotometry and pulse radiolysis. The replacements of these side chains inhibited steps in the catalysis as much as 50-fold; in addition, they altered the gating between catalysis and formation of a peroxide complex to yield a more product-inhibited enzyme. The replacement of both Tyr34 and Trp123 in a double mutant showed that these two residues interact cooperatively in maintaining catalytic activity. The crystal structure of Y34F/W123F human MnSOD at 1.95 Å resolution suggests that this effect is not related to a conformational change in the side chain of Gln143, which does not change orientation in Y34F/W123F, but rather to more subtle electronic effects due to the loss of hydrogen bonding to the carboxamide side chain of Gln143. Wild-type MnSOD containing Trp123 and Tyr34 has approximately the same thermal stability compared with mutants containing Phe at these positions, suggesting the hydrogen bonds formed by these residues have functional rather than structural roles.

Human manganese superoxide dismutase (MnSOD)[1] is a homotetramer composed of 22 kDa subunits each containing one active site (*1*, *2*). Initial studies of human manganese superoxide dismutase show a trigonal bipyramidal geometry about the active site manganese, the ligands consisting of three histidines, an aspartate residue, and one solvent molecule (*1*). In the catalytic disproportionation of superoxide, MnSOD cycles between the Mn(III) and Mn(II) states to produce oxygen and hydrogen peroxide. Catalysis is rapid with a k_{cat} near 4×10^4 s^{-1} and a k_{cat}/K_m near diffusion control at 8×10^8 M^{-1} s^{-1} (*3*). Addition of substrate also initiates the appearance within milliseconds of an inhibited form; after a brief initial burst, catalytic decay of superoxide is characterized by zero-order kinetics in which a peroxide-inhibited form plays a significant role (*3*, *4*). This enzymatic form is proposed to be an inner-sphere, end-on or side-on, peroxo complex (*4*, *5*), and its visible absorption spectrum resembles that of the azide-inhibited form of MnSOD (*6*, *7*).

Beyond the inner sphere of ligands are several residues that are part of an extensive hydrogen bond network, necessary for rapid catalytic turnover (*8*). This work focuses upon the function of Trp123 and its interaction with Tyr34, two residues which form hydrogen bonds to the critical Gln143 residue, the side chain of which is hydrogen bonded to the solvent molecule that is a ligand to the manganese. Replacement of Gln143 with Asn in human MnSOD results in a decrease of 3 orders of magnitude in k_{cat}/K_m for superoxide decay (*9*). Previous studies have investigated the structural, spectroscopic, and catalytic role of Tyr34 in MnSOD (*10*, *11*).

In this work, we estimate the role of the hydrogen bonds between Gln143, Tyr34, and Trp123. A crystal structure of the double mutant Y34F/W123F Mn(III)SOD shows no significant structural consequences beyond the removal of these hydrogen bonds. Moreover, these replacements do not

[†] This work was supported by National Institutes of Health Grants GM54903 (to D.N.S.) and GM48495 (to J.A.T.) and an American Lung Association grant (to A.H.S.). The pulse radiolysis work was carried out at Brookhaven National Laboratory under Contract DE-AC02-98CH108816 with the U.S. Department of Energy and supported by its Division of Chemical Sciences, Office of Basic Energy Sciences.

[‡] Coordinates for Y34F/W123F human MnSOD were deposited in the Protein Data Bank as entry 1SZX.

* To whom correspondence should be addressed: Box 100267, Health Center, University of Florida, Gainesville, FL 32610-0267. Phone: (352) 392-3556. Fax: (352) 392-9696. E-mail: silvermn@college.med.ufl.edu.

[§] University of Florida.

[∥] The Scripps Research Institute.

[⊥] Brookhaven National Laboratory.

[@] University of Toronto.

[1] Abbreviations: MnSOD, manganese superoxide dismutase; SHIE, solvent hydrogen isotope effect; PCR, polymerase chain reaction; MOPS, 3-(*N*-morpholino)propanesulfonic acid; TAPS, *N*-tris(hydroxymethyl)methyl-3-aminopropanesulfonic acid; CHES, 2-(*N*-cyclohexylamino)ethanesulfonic acid; CAPS, 3-cyclohexylamino-1-propanesulfonic acid; CA II, carbonic anhydrase II.

10.1021/bi049888k CCC: $27.50
Published on Web 05/11/2004

have large effects on the major thermal unfolding transition of MnSOD near 90 °C. However, the replacements of Tyr34 and Trp123 with Phe decreased the catalytic activity of MnSOD and resulted in an enzyme that was more product-inhibited than the wild type. Both Tyr34 and Trp123 appear to act cooperatively in this effect on catalytic activity.

MATERIALS AND METHODS

Site-Directed Mutagenesis. Human manganese superoxide dismutase cDNA (cDNA sequence published in ref *12*) was amplified via PCR using two oligonucleotides, 5′-GCATATGAAGCACAGCCTCC-3′ and 5′-GGAGATCTCAGCATAACGATC-3′. The human MnSOD-containing plasmid pHMNSOD4 (ATCC 59947) was subcloned into TA cloning vector pCRII (Invitrogen Corp.). Four primers were used to generate the W123F mutant. The first pair of primers was used to regenerate the coding region: 5′-CGCTAGTAATCATTTCATGAAGCACAGCCT-3′ (primer 1) and 5′-CGCCAAAACAGCCAAGCTTGCATGCCTGCA-3′ (primer 2). The second pair of primers (primers 3 and 4) differed for each mutant, and served as complementary internal primers encoding the desired mutation (underlined). For the site-directed mutant W123F, the second pair of primers was 5′-AAGGCTCAGGTTTTGGTTGGCTTG-3′ (primer 3) and 5′-CAAGCCAACCAAAACCTGAGCCTT-3′ (primer 4). To generate the Y34F/W123F site-directed mutant, the Y34F human MnSOD cDNA was used as the template, using the same primers that were used for the W123F site-directed mutant. Four other substitutions at the W123 site were made, including Ala, Val, His, and Tyr. In one PCR, primers 1 and 4 were used to generate the 5′ half of the coding sequence, while in a separate PCR, primers 2 and 3 were used to generate the 3′ half of the coding sequence. The products of the first two reactions were gel purified using the QIAgen gel extraction kit (QIAgen Corp.) and then used as templates along with primers 1 and 2 in a third reaction to generate the complete coding sequence containing the mutation of interest. The PCR product was then cut with *Bsp*HI and *Pst*I and cloned into the pTRC99a expression vector (Pharmacia Corp.). The *Bsp*HI site, located at the N-terminal end of the protein, was annealed to the compatible *Nco*I site in the pTRC99a vector, while the *Pst*I site at the C-terminal end was annealed to the *Pst*I site in pTRC99a. The sequences of all mutants generated in this manner were verified by DNA sequence analysis.

Protein Expression and Purification. The pTRC99a plasmid containing the mutated human MnSOD coding sequence was transformed into *Sod A*$^-$/*Sod B*$^-$ null mutant *Escherichia coli* strain QC774 (*13*). The mature protein was expressed with an extra methionine at the N-terminal end of the protein. The bacterial medium was supplemented with 660 μM $MnCl_2$ during protein expression. Cells were harvested by centrifugation, lysed, heat-treated at 60 °C, and then extensively dialyzed against the appropriate buffer. The enzyme was purified via FPLC on a Q-Sepharose anion-exchange resin (Amersham Biosciences), and when necessary by gel filtration on a Sephacryl S-300 column. Purity was determined by SDS−polyacrylamide gel electrophoresis, where one intense band at 22 kDa indicated the presence of the monomer form of MnSOD. After the buffer had been exchanged, the enzyme concentration was determined by UV spectrophotometry (ϵ_{280} = 40 500 M^{-1} cm^{-1}). Total manganese, determined by flame atomic absorption spectroscopy, was used to determine the active enzyme concentration. Metal contents were typically between 60 and 80% of the total protein.

Pulse Radiolysis. All pulse radiolysis experiments were performed at Brookhaven National Laboratory, using the 2 MeV van de Graaff accelerator as described by Hearn et al. (*14*). All spectra were obtained on a Cary 210 spectrophotometer with the path length set to 2.1 cm. Solutions at 25 °C contained enzyme, 30 mM sodium formate, 50 μM EDTA, and one of the following buffers (at 2 mM) depending upon the pH of the experiment: MOPS at pH 6.5−7.5, TAPS at pH 8.0−8.5, CHES at pH 9.0−9.5, or CAPS at pH 10.0−10.5. Production of up to 30 μM superoxide radicals upon pulsing the aqueous air-saturated solution occurred according to the mechanisms described by Schwarz (*15*).

Differential Scanning Calorimetry. Studies were performed using a Nano differential scanning calorimeter (Calorimetry Sciences, American Forks, UT). Protein samples of the mutants and wild-type MnSOD were prepared at a concentration of 1 mg/mL in potassium phosphate (20 mM, pH 7.8). An identical solution without protein was used as a reference. Both the sample and reference were degassed at 4 °C before scanning from 10 to 110 °C at 1 °C/min. The baseline and change in specific heat (ΔC_p) upon denaturation were corrected as described previously (*16*, *17*). The transitions in the differential scanning calorimetry profile were fit assuming a non-two-state, single-component mode (*18*) using Origin (Microcal Software, Northampton, MA). The $\Delta\Delta G$ is the ΔG of the mutant calculated at the appropriate transition temperature (T_m) of the wild-type protein, assuming a constant ΔH ($\Delta C_p = 0$). All $\Delta\Delta G$ values are in kilocalories per mole of tetramer and were calculated using the van't Hoff enthalpy and T_m from the best fits of the transitions. The estimated error of the transition temperature was less than 0.3 °C.

Stopped-Flow Spectrophotometry. The method of McClune and Fee (*19*) was used to measure the zero-order rate constant k_0/[E]. Potassium superoxide (Aldrich) and an equimolar amount of 18-crown-6 ether used to increase solubility were dissolved in dry DMSO. A dual mixing stopped-flow spectrophotometer (Applied Photophysics, SX18.MV) was used to follow the decrease in the absorption of superoxide at 250 nm [ϵ_{250} = 2000 M^{-1} cm^{-1} (*20*)]. Sequential dilutions were used; first, superoxide in DMSO in a 250 μL syringe was mixed in a 1:10 ratio with an aqueous solution at pH 11 containing 2 mM CAPS and 1 mM EDTA. After a 500 ms delay, this solution was rapidly mixed in a 1:1 ratio with a solution containing 4 μM enzyme, 200 mM CAPS, and 1 mM EDTA at pH 10.5. The final concentration of DMSO was 4.5 vol %. The average instrumental dead time was 4 ms. The mean of six to eight catalytic traces was fit to the sum of zero-order (catalyzed) and second-order (uncatalyzed) processes.

Crystallography. Orthorhombic crystals of Y34F/W123F MnSOD were grown by vapor diffusion from a solution consisting of 26 mg/mL protein, buffered in 25 mM K_2HPO_4 (pH 7.8) and 22% poly(ethylene glycol) (PEG) 2000 monomethyl ether. A flash-frozen single crystal, supplemented with 20% ethylene glycol cryoprotectant in its mother liquor, was used for X-ray diffraction data collection at 100

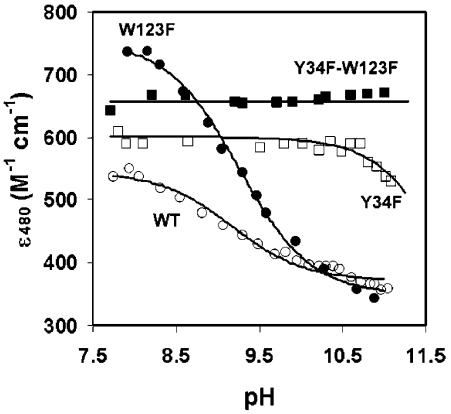

FIGURE 1: Change in molar absorptivity at 480 nm as a function of pH for wild-type (○), W123F (●), Y34F (□), and Y34F/W123F (■) human MnSOD. A single ionization with a pK_a of 9.2 ± 0.1 was used to fit the data for W123F and wild-type human MnSOD.

K. A data set was collected to 1.95 Å on a Q210 ADSC CCD detector at beamline 5.0.2 of the Advanced Light Source, Lawrence Berkeley National Laboratory (Berkeley, CA). The data were indexed and merged with Denzo and scaled with Scalepack (*21*). The crystal belonged to space group $P2_12_12$ and had the following unit cell dimensions: a = 73.9 Å, b = 75.6 Å, and c = 68.4 Å. The data set was 99.0% complete [100% for the highest-resolution shell (2.02−1.95 Å); 27 941 unique reflections measured] with an R_{sym} of 9.3% (25.3% for the highest-resolution shell). The data have an overall $I/\sigma I$ of 45.5 with an $I/\sigma I$ in the highest-resolution shell of 8.2 and a crystal mosaicity of 0.8°. Phases were obtained by molecular replacement against the wild-type human MnSOD structure in Crystallography and NMR Systems, version 1.1 (*22*) (CNS). The structure was fit against CNS-calculated $2F_o - F_c$, $F_o - F_c$, and composite omit electron density maps in the Xfit module of XtalView (*23*) and refined in CNS. The structure was refined to an R_{work} of 24.2% and an R_{free} (*24*) of 29.0% (with 5% of the reflections flagged for the test set). Coordinates were deposited in the Protein Data Bank as entry 1SZX.

RESULTS

Visible Spectrophotometry. The visible spectrum of human MnSOD shows a broad absorption with a maximum at 480 nm (*3*). The pH profile of the molar absorptivity at 480 nm (ϵ_{480}) can be fit to an ionization with a pK_a of 9.2 ± 0.1 (Figure 1; see also refs *3* and *10*). This fit does not include a very small decrease in this extinction coefficient above pH 10.5 that may indicate a minor influence of a second ionization. The absorption spectrum of W123F MnSOD exhibited a value of ϵ_{480} at pH <10 larger than that of the wild type; however, upon titration, it showed the same pK_a of 9.2 ± 0.1. In contrast, the pH profile of Y34F/W123F exhibited little change in ϵ_{480}, while data for Y34F showed a decrease in ϵ_{480} at pH >10.5 [Figure 1 (*10*)]. The manganese specificity of W123F was unchanged from that of the wild type or Y34F; typically, the manganese content of Y34F/W123F was 80% per monomer, while the iron content was less than 1% per monomer.

Catalysis. From the change in absorbance of superoxide at 250 nm, we measured the progress curves for the decay of superoxide catalyzed by wild-type and mutant human MnSOD by stopped-flow spectrophotometry. These curves for W123F and Y34F/W123F MnSOD could be fit to the sum of zero-order and second-order (uncatalyzed) processes, but were dominated by the zero-order component that has been associated with product inhibition of MnSOD (*4*, *14*). Typical data for W123F MnSOD show the predominant zero-order decay (Figure 2). The zero-order rate constants k_0/[E] were smaller by ~3−8-fold for all of the variants of this study compared with that of wild-type MnSOD (Table 1), demonstrating greater product inhibition during catalysis.

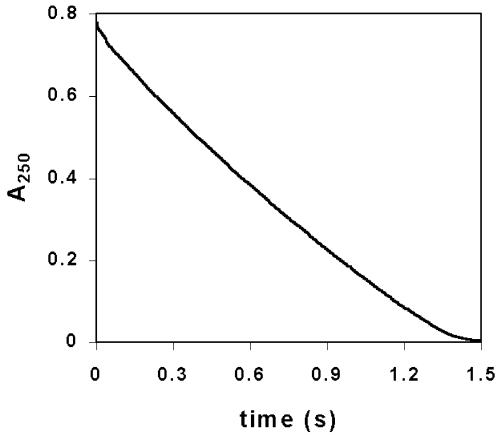

FIGURE 2: Decrease in A_{250} due to the decay of superoxide (ϵ_{250} = 2000 M^{-1} cm^{-1}) catalyzed by 2 μM W123F human MnSOD measured by stopped-flow spectrophotometry. The solution contained 100 mM CAPS, 500 μM EDTA (pH 10.5), and 4.5 vol % DMSO, with an initial concentration of superoxide of 390 μM. The solid line is a fit to the sum of a zero-order process with a k_0/[E] of 76 s^{-1} and an uncatalyzed, second-order rate constant of 440 M^{-1} s^{-1}.

A simplified kinetic scheme (eqs 1−4) has been used to describe catalysis by MnSOD (*14*, *25*). This scheme is modified here to reflect the observation that MnSOD takes up a proton upon reduction of the metal, shown as Mn(II)SOD(H^+) in eq 1; in addition, the protonated site is suggested to be a solvent ligand of the metal (*26*). Here Mn(III)(O_2^{2-})SOD(H^+) represents the inhibited complex.

$$\mathrm{Mn(III)SOD} + \mathrm{O_2^{\bullet -}} \xrightarrow{k_1(+\mathrm{H^+})} \mathrm{Mn(II)SOD(H^+)} + \mathrm{O_2} \quad (1)$$

$$\mathrm{Mn(II)SOD(H^+)} + \mathrm{O_2^{\bullet -}} \xrightarrow{k_2(+\mathrm{H^+})} \mathrm{Mn(III)SOD} + \mathrm{H_2O_2} \quad (2)$$

$$\mathrm{Mn(II)SOD(H^+)} + \mathrm{O_2^{\bullet -}} \xrightarrow{k_3} \mathrm{Mn(III)(O_2^{2-})SOD(H^+)} \quad (3)$$

$$\mathrm{Mn(III)(O_2^{2-})SOD(H^+)} \xrightarrow{k_4(+\mathrm{H^+})} \mathrm{Mn(III)SOD} + \mathrm{H_2O_2} \quad (4)$$

Two stages of the catalytic cycle (eqs 1 and 2) are treated as irreversible, justified by favorable equilibrium constants for formation of products. The formation and dissociation of the product-inhibited complex are represented in eqs 3 and 4. Estimates of rate constants k_1−k_4 were made by observation of the rate of change of absorbance of superoxide and of enzyme species in single-turnover experiments after introduction of superoxide by pulse radiolysis (*14*). Rate

Table 1: Zero-Order Rate Constant k_0/[E] Describing a Product-Inhibited Region of Catalyzed Decay of Superoxide and Second-Order Rate Constants k_1 and k_2 for Steps in the Catalytic Mechanism (eqs 1 and 2) for Human Wild-Type MnSOD and Site-Specific Mutants

enzyme	k_0/[E] (s^{-1})[a]	k_1 (nM^{-1} s^{-1})[b]	k_2 (nM^{-1} s^{-1})[b]
wild-type	220	1.5 ± 0.1[c]	1.1 ± 0.1[c]
Y34F	26	0.55 ± 0.03	<0.02
W123F	75	0.76 ± 0.05	<0.02
Y34F/W123F	58	0.66 ± 0.06	<0.02
W161F	50	0.30 ± 0.08[c]	<0.01[c]

[a] Data taken from stopped-flow measurements at pH 8.0 and 20 °C with 100 mM TAPS, 500 μM EDTA, and 2 μM enzyme. The error is less than 10% for each value. [b] From pulse radiolysis with conditions as described in the legend of Figure 3 (pH 7.5). Values are the average and standard deviations of at least three measurements. [c] Rate constant for wild-type MnSOD and W161F MnSOD at pH 8.2 and 25 °C taken from ref *14*.

constant k_1 was estimated from the decrease in absorbance at 480 nm of the oxidized enzyme. k_2 typically is difficult to estimate in mutants of MnSOD that are strongly product inhibited due to the rapid emergence of the product-inhibited form (*14*). k_3 was estimated from the appearance of a peak absorption at 420 nm characteristic of the product-inhibited form. k_4 was determined by observing the increase at 480 nm and the concurrent decrease at 420 nm corresponding to decay of the product-inhibited complex.

Typical single-turnover experiments beginning with Y34F/W123F Mn(II)SOD showed the first-order increase in absorbance at 420 nm on a microsecond time scale corresponding to formation of the product-inhibited complex (eq 3) (Figure 3A), and the subsequent increase in absorbance at 480 nm on a millisecond time scale resulting from the dissociation of the product-inhibited complex and appearance of uncomplexed Mn(III)SOD (eq 4) (Figure 3B). The replacement of Tyr34 and Trp123 with Phe caused modest reductions of ~2−3-fold in rate constants k_1 and k_3; the double mutant exhibited roughly the same magnitude of decrease as the wild type (Tables 1 and 2). Values of k_4 also decreased as much as 4-fold with these replacements (Table 2).

An accurate measurement of k_2 was not possible in these highly product-inhibited mutants of MnSOD since changes in absorption at 420 nm corresponding to the inhibited pathway (eq 3) dominate over smaller changes at 480 nm which represent eq 2 of the catalytic cycle. Using the kinetic simulation of KINSIM (*27*), we fit the superoxide decay traces obtained from pulse radiolysis to estimate a range of values for k_2 that would be consistent with the data. In this simulation, values of k_1, k_3, and k_4 determined experimentally (Tables 1 and 2) were held constant while k_2 was varied until good agreement was seen between modeled and experimentally observed progress curves for the catalyzed decay of superoxide. For the mutants of Table 1, an upper limit of 0.02 nM^{-1} s^{-1} for k_2 could be estimated (Table 1).

The pH profile of k_1 (eq 1) for wild-type human MnSOD was independent of pH up to pH 9.5; at higher pHs, it showed a decrease, the pK_a of which is estimated to be >10.0 (Figure 4). In contrast, the pH profiles of k_1 for Y34F, W123F, and the double mutant were very similar not only in magnitude but also in pK_a, 9.5 ± 0.2 (shown for Y34F/W123F in Figure 4). The pH profiles of k_3 (eq 3) for the wild type, Y34F,

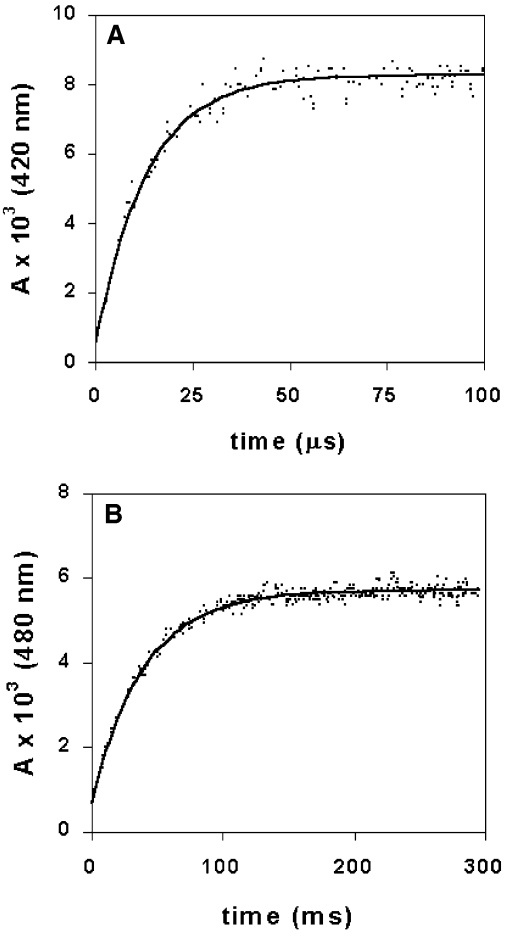

FIGURE 3: (A) Increase in the absorbance at 420 nm of 120 μM Y34F/W123F Mn(II)SOD over microsecond time scales after pulse radiolysis generated 6.7 μM $O_2^{\bullet-}$ in solution. The enzyme was reduced with H_2O_2 prior to pulsing. Solutions contained 30 mM formate, 50 μM EDTA, and 2 mM MOPS at pH 7.5 and 25 °C. The solid line is a fit to a first-order process corresponding to a k_3 of 0.64 ± 0.06 nM^{-1} s^{-1}. (B) Increase in the absorbance at 480 nm of 120 μM Y34F/W123F MnSOD over millisecond time scales after pulse radiolysis generated 3.2 μM $O_2^{\bullet-}$. Solution conditions were identical to those described for panel A. The solid line is a fit to a first-order process corresponding to a k_4 of 25 ± 1 s^{-1}.

Table 2: Rate Constants k_3 and k_4 and Their Solvent Hydrogen Isotope Effects for Steps in the Formation and Dissociation of the Product-Inhibited Complex (eqs 3 and 4) for Human Wild-Type MnSOD and Site-Specific Mutants[a]

enzyme	k_3 (nM^{-1} s^{-1})	$^Dk_3$[b]	k_4 (s^{-1})	$^Dk_4$[b]
wild-type[c]	1.1 ± 0.1	1.2 ± 0.2	120 ± 10	1.7 ± 0.2
Y34F	0.46 ± 0.05	1.1 ± 0.2	52 ± 3	1.8 ± 0.2
W123F	0.64 ± 0.08	1.0 ± 0.2	79 ± 4	1.8 ± 0.2
Y34F/W123F	0.70 ± 0.09	1.0 ± 0.2	27 ± 2	1.9 ± 0.2
W161F[c]	0.46 ± 0.04	1.0 ± 0.1	33 ± 3	2.2 ± 0.2

[a] Conditions as described in the legend of Figure 3 (pH 7.5). Values are the average and standard deviations of at least three measurements. [b] Solvent hydrogen isotope effects are indicated with a superscript D, as in $^Dk_3 = (k_3)_{H_2O}/(k_3)_{D_2O}$. [c] Rate constants for wild-type MnSOD and W161F MnSOD at pH 8.2 and 25 °C taken from ref *14*.

W123F, and the double mutant were nearly identical to those of k_1 for these enzymes (Figure 5). The values of k_4 (eq 4) for wild-type and Y34F MnSOD showed no pH dependence over the pH range depicted in Figure 6. The pH profiles of k_4 for the two mutants containing W123F have a pH dependence consistent with a pK_a near 9.2 (Figure 6). The data for W123F and Y34F/W123F MnSOD were obtained

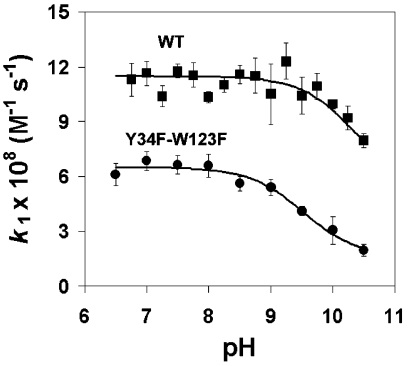

FIGURE 4: Dependence of k_1 on pH for Y34F/W123F (●) and wild-type human MnSOD (■). Solutions at 25 °C contained 120 μM Y34F/W123F, 30 mM formate, 50 μM EDTA, and one of the following buffers (2 mM): MOPS at pH 6.5−7.5, TAPS at pH 8.0−8.5, CHES at pH 9.0−9.5, or CAPS at pH 10.0−10.5. Data for wild-type MnSOD were taken from ref *14*. Each data point is the mean and standard deviation of 6−12 measurements. The data for Y34F/W123F were fit to a single ionization with a pK_a of 9.5 ± 0.2; wild-type data were consistent with a pK_a of >10.0.

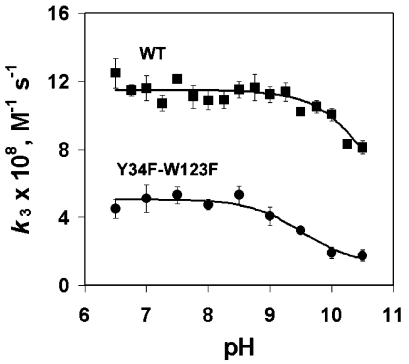

FIGURE 5: Dependence of k_3 on pH for Y34F/W123F (●) and wild-type human MnSOD (■). Solution conditions were identical to those described in the legend of Figure 4. Data for wild-type MnSOD were taken from ref *14*. Each data point is the mean and standard deviation of 6−12 measurements. The data for Y34F/W123F were fit to a single ionization with pK_a of 9.5 ± 0.2; wild-type data were consistent with an ionization with a pK_a of >10.0.

following reduction of the enzyme with hydrogen peroxide. Values of k_4 for these two mutants did not depend on the concentration of peroxide used except at pH ~10, and the data that had a significant peroxide dependence are not reported.

Experiments in H_2O and D_2O (98%) were carried out to estimate the solvent hydrogen isotope effect (SHIE) on rate constants k_3 and k_4. For the three mutant MnSODs and the wild type, k_3 displayed a SHIE indistinguishable from unity (Table 2). However, an SHIE near 2 was observed for k_4 for each of the mutants and the wild type.

Calorimetry. Differential scanning calorimetry was used to determine the thermal stability of the human wild-type MnSOD and variants at positions 34 and 123 (Table 3). The changes in the main unfolding transition temperature T_m and $\Delta\Delta G$ were modest. The values of $\Delta\Delta G$ were calculated assuming $\Delta C_p = 0$ since it is difficult to measure ΔC_p accurately and incorporating ΔC_p into the calculation for $\Delta\Delta G$ has only a small effect when changes in stability are small. The main unfolding transition (T_m) of the wild-type enzyme with Gln143 hydrogen bonded to both Tyr34 and Trp123 was 90.7 °C. Replacing Trp123 with Phe had no effect on stability, while replacing Tyr34 with Phe increased

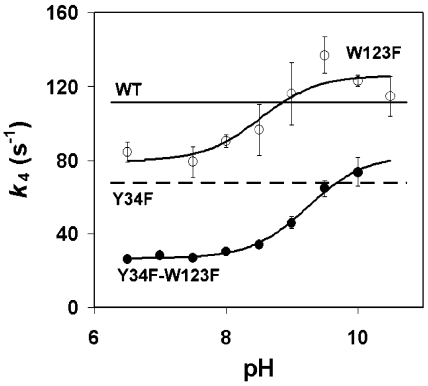

FIGURE 6: Dependence of k_4 on pH for Y34F/W123F (●) and W123F (○) MnSOD. Solution conditions were identical to those described in the legend of Figure 4. Each data point is the mean and standard deviation of 6−12 measurements. A single ionization was fit to the data for Y34F/W123F with a pK_a of 9.3 ± 0.1 and to W123F with a pK_a of 9.1 ± 0.2. The values of k_4 for wild-type (represented by the solid line, points omitted) and Y34F (dashed line) human MnSOD are invariant over this pH range and are given in Table 1.

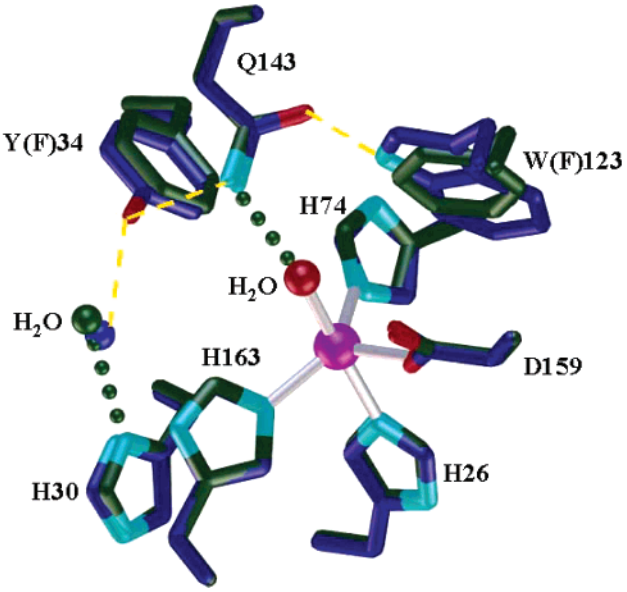

FIGURE 7: Crystal structure of the active site of human Y34F/W123F MnSOD (black) superimposed upon wild-type human MnSOD (blue) (*1*). Hydrogen bonds connecting Tyr34, Gln143, and Trp123 are shown in orange for the wild type but cannot form in the mutant.

Table 3: Unfolding Transition Temperatures of Wild-Type Human MnSOD and Mutants at Positions 34 and 123

MnSOD	T_m (°C)[a]	$\Delta\Delta G$ (kcal/mol of tetramer)
wild-type	90.7	–
Y34F	94.2	1.2
W123F	90.6	0
Y34F/W123F	88.7	−0.7

[a] The standard deviation of T_m was estimated to be 0.3 °C.

stability (ΔT_m = 3.5 °C; Table 3). The substitution of phenylalanine at both positions in the double mutant (Y34F/W123F) was destabilizing (ΔT_m = −2.0 °C). Substitutions at position 123 that could not be purified and were presumably unstable included Ala, Val, His, and Tyr.

Crystallography. Like the wild-type enzyme, the W34F/W123F MnSOD mutant crystallized in space group $P2_12_12$.

The asymmetric unit contains a homodimer, and the biologically relevant tetramer is formed from a crystallographic 2-fold symmetry axis. The W34F/W123F subunit fold and tetramer assembly are well-defined in the 1.95 Å electron density maps, and are very similar to the previously determined wild-type structure; superposition of the two mutant asymmetric subunit structures onto the two wild-type asymmetric subunits gave an average root-mean-square deviation for all 198 Cα atoms of 0.34 Å. Minimal changes have occurred to the position, orientation, and bonding distances of residues and water molecules of the substrate access funnel and active site (active site region in Figure 7). The phenyl rings of Phe34 and Phe123 appear to be superimposed on the phenol and indole rings of the wild type at these positions (Figure 7). Moreover, the water structure in the active site and substrate access funnel has not changed in the W34F/W123F double mutant compared with that in the Y34F mutant and wild-type structures. The position of the carboxamide group of Gln143 appears to be the same as in the wild-type and Y34F structures; however, the double mutation Y34F/W123F has eliminated two hydrogen bonds to the side chain of Gln143, and we cannot comment on whether the orientation of this side chain has rotated 180° with respect to the wild type. Instead, the main structural alteration in the Y34F/W123F double mutation is the removal of the Tyr34 and Trp123 hydrogen bonds to Gln143.

DISCUSSION

The side chain of Gln143, a conserved residue in MnSOD, forms a hydrogen bond with the manganese-bound solvent [Figure 7 (*1*)], functions to maintain the catalytic activity (*9*, *28*), and by influencing the pK_a of the metal-bound water fine-tunes the redox potential at the metal (*29*). The side chains of Tyr34 and Trp123 form hydrogen bonds with the carboxamide side chain of Gln143. In other metalloenzymes, such third-shell ligands serve to orient second-shell ligands for catalysis and influence the pK_a of the metal-bound water [i.e., Glu106 in carbonic anhydrase (*30*)]. In this work, we have replaced Tyr34 and Trp123 through site-specific mutagenesis to examine their functional and structural role and their possible interaction. This work complements earlier studies of the replacement of Tyr34 in MnSOD (*10*, *11*).

The 1.95 Å crystal structure of Y34F/W123F human Mn(III)SOD was very structurally similar to the wild type (Figure 7). In the mutant, the carboxamide of Gln143 has lost its hydrogen bonds to residues 34 and 123; however, the side chains of Phe34 and Phe123 superimpose very closely on the corresponding phenol and indole rings of residues 34 and 123, respectively, in the wild-type enzyme. Significantly, there appears to be no change in the position of the carboxamide group of Gln143 in this double mutant compared with the wild type. In addition, the trigonal bipyramidal configuration of the ligands of the metal is the same in the mutants and wild type (Figure 7). Therefore, the prominent structural change in Y34F/W123F compared with the wild type is the absence of the two hydrogen bonds to Gln143.

The pH profiles of the visible absorption maximum at 480 nm for wild-type and Y34F Mn(III)SOD are consistent with Tyr34 as the source of the pK_a near 9.2 (Figure 1), as suggested by Hsu et al. (*3*) on the basis of similar data and determined by Maliekal et al. (*29*) on the basis of more detailed spectroscopic studies. This pK_a near 9.2 for human Mn(III)SOD has also been attributed to the binding of OH^- to the metal on the basis of comparisons of the spectroscopic properties of MnSOD and FeSOD (*11*). The replacement of Trp123 with Phe did not influence this pK_a near 9.2 attributed to Tyr34 (Figure 1); this is one property for which Tyr34 and Trp123 in MnSOD do not interact. Moreover, the replacement of Trp123 with Phe did not alter the selectivity of this binding site for manganese; the iron content of the purified mutant enzyme was very low, near 1% of binding sites for metal at the active site.

Though not essential to catalysis, Trp123 contributes significantly to the catalytic capacity. Rate constants for individual steps in a simplified catalytic mechanism (eqs 1−4) showed that replacement of Trp123 with Phe resulted in a 2−3-fold decrease in rate constants k_1 and k_3, and an at least 50-fold decrease in k_2 (Table 1). The observation that $k_2 \ll k_3$ was made for the single mutants (Y34F and W123F) and the corresponding double mutant and is a significant source of the greater product inhibition observed in the mutants compared with the wild type. That is, the magnitude of k_2 compared with that of k_3 determines the gating into the product-inhibited form, and a very significant result of each of the mutants of Table 1 is a major change in this gating. In fact, so prominent is this change in gating and the resulting inhibition that the progress curve for catalysis by W123F MnSOD (Figure 2) can be explained entirely by the product-inhibited form (and the uncatalyzed dismutation). The enhanced product inhibition in the mutants was observed as a 3−8-fold decrease in the rate constant k_0/[E] for the zero-order region of catalysis compared with that of the wild type (Table 1). Results very similar to these were obtained for the replacement of Trp161 with Phe (Table 1) (*14*). These residues (Tyr34, Trp123, and Trp161) are all components of the active site cavity with their aromatic side chains within 6 Å of the metal. They appear to maintain the pathway of catalysis containing the oxidation of the manganese (eq 2).

It is remarkable that the magnitudes (Tables 1 and 2) and pH dependencies (Figures 4 and 5) of k_1 and k_3 were very similar, nearly identical, for each of the single and double mutants as well as for wild-type MnSOD. The first conclusion from this observation is that the catalytic steps represented by k_1 and k_3 (eqs 1 and 3, respectively) appear not to be sensitive to the difference in the formal charge on the metal, since k_1 proceeds with the metal oxidized and k_3 proceeds with the metal reduced. Miller et al. (*26*) have observed that MnSOD takes up a proton upon reduction of the metal and have interpreted their data as being consistent with protonation at the aqueous ligand of the metal. Thus, the oxidized and reduced forms of the active site may be P($Mn^{3+}OH^-$) and P($Mn^{2+}H_2O$), respectively (where P is the protein). Clearly, the delocalization of charge into the ligands as well as the formal neutralization of charge on the oxidized metal by hydroxide indicates that the electrostatics at the active site may be similar for k_1 and k_3.

We note that the mutations in which both Tyr34 and Trp123 are replaced with Phe have the same effect, greatly enhancing product inhibition. This occurs by altering the gating between catalysis (k_2) and inhibition (k_3); each mutation (Y34F and W123F) as well as the double mutant

decreases k_2 with little effect on k_3 (Tables 1 and 2). We know that the steps described by k_2 clearly involve proton transfer for formation of product H_2O_2; moreover, these proton transfer steps contribute to rate as indicated by the H/D isotope effect near 2 on the maximal velocity of catalysis by MnSOD (*4*). The gating between the steps of k_2 and k_3 can be described in terms of proton accessibility at the active site with the proton donated by the metal-bound water (*31*). In this context, the significant decreases seen in k_2 for the mutants of Table 1 most likely indicate the effects of these mutations on the accessibility of protons in the reactions of eq 2. If proton transfer proceeds predominantly to O_2^{2-}, then formation of product hydrogen peroxide is promoted and catalysis occurs. However, if proton transfer is slow or occurs at another site, such as the side chain of Asp159 rather than to O_2^{2-} (*31*), then this peroxo ligand forms the product-inhibited complex. Hence, the data suggest that the enhanced product inhibition in Y34F/W123F MnSOD arises from altered gating between catalysis and inhibition, a gating that is caused by changes in the proton transfer pathway. These results suggest a significant role of the side chains of Tyr34 and Trp123 is to extend to the active site a network of hydrogen bonding, the ultimate effect of which is to provide protons for formation of the product hydrogen peroxide.

The rate constant for dissociation of the inhibited complex k_4 for both single and double mutants containing the replacement of Trp123 with Phe exhibited a pH dependence with a pK_a near 9.2 and a maximum at high pH (Figure 6). Wild-type and Y34F MnSOD exhibited no pH dependence in this parameter. Similar behavior in k_4 was observed for the W161A mutant (*14*). Hence, the deprotonated form of an ionizable group facilitates dissociation of the product-inhibited complex in mutants containing Phe123. The source of this pH variation is not apparent since there appear to be minimal changes in the active site structure of Y34F/W123F MnSOD (Figure 7), but the source is not the ionization of Tyr34 as shown in Figure 6. Since proton transfer contributes to the rate in k_4 as suggested by a solvent hydrogen isotope effect of 2 (Table 2), the ionization could affect the proton transfer pathway to the peroxo complex at the manganese. These properties for k_4 are different from those for k_1 and k_3, demonstrating the unique and proton transfer-dependent steps of k_4.

To investigate possible interactions between Y34 and W123 in catalysis, we constructed the double mutant. Interestingly, in Y34F/W123F MnSOD, rate constants k_1 and k_3 were close to the same as in the single mutants (Tables 1 and 2). That is, the kinetic effects due to either mutation represent a threshold, and mutation at the other site does not enhance the effect further. Another manifestation of this is that the apparent kinetic pK_a values obtained from k_1 and k_3 (Figures 4 and 5) are identical for the two single mutants and the double mutant at a pK_a of 9.5 ± 0.2, whereas the value of the pK_a obtained for the wild type, although uncertain, appears at p$K_a > 10.0$. This indicates an interaction between Tyr34 and Trp123 for these catalytic steps; $\Delta G_{1+2} = \Delta G_1 = \Delta G_2$ which indicates a cooperative interaction in which ΔG_{1+2} represents the free energy change for catalysis by the double mutant and ΔG_1 and ΔG_2 represent the change for single mutants (*32*). Our data suggest that loss of the hydrogen bond from Trp123 to Gln143 is as detrimental to activity as loss of the hydrogen bond from Tyr34. These results, viewed with the very minor structural changes seen in the Y34F/W123F mutant compared to the wild type (Figure 7), suggest the loss of a hydrogen bond to Gln143 as a cause of the decrease in k_1 and k_3, rather than a conformational change.

The mutants of Table 3 have thermal stabilities approximately the same as that of the wild type; hence, neither Tyr34 nor Trp123 flanking Gln143 is stabilizing compared to Phe at these positions. The relatively small changes in the unfolding transition upon substitution of Phe at positions 34 and 123 suggest the hydrogen bonds from these residues to Gln143 are more likely functional rather than structural; this is in agreement with the catalytic activity being reduced but the stability rather unchanged in each mutant. However, we point out that mutants of MnSOD with residues other than Phe at position 123 were too unstable to study, suggesting that there may be a significant structural role for Trp123.

In summary, a significant role of Trp123 in human MnSOD is in maintaining the gating between catalysis and product inhibition. As found when Tyr34 was replaced with Phe (*10*) and Trp161 was replaced with Phe (*33*), we found that the extent of inhibition by a peroxo complex of the metal overwhelmed catalysis when Trp123 was replaced with Phe. It is possible that some degree of product inhibition is desirable for preventing cellular overload of product H_2O_2 (*34*); however, compared with phenylalanine, Trp123 and Tyr34 of the wild type function in significant part to maintain catalysis and slow product inhibition in MnSOD.

ACKNOWLEDGMENT

We thank Harold Frey for calorimetry studies and Max Iurcovich for excellent technical assistance.

REFERENCES

1. Borgstahl, G. E. O., Parge, H. E., Hickey, M. J., Beyer, W. F., Hallewell, R. A., and Tainer, J. A. (1992) The structure of human mitochondrial manganese superoxide dismutase reveals a novel tetrameric interface of two 4-helix bundles, *Cell 71*, 107−118.
2. Sorkin, D. L., and Miller, A. F. (1997) Superoxide Dismutases: A Molecular Perspective, *Comments Mol. Cell. Biophys. 9*, 1−48.
3. Hsu, J.-L., Hsieh, Y., Tu, C. K., O'Connor, D., Nick, H. S., and Silverman, D. N. (1996) Catalytic properties of human manganese superoxide dismutase, *J. Biol. Chem. 271*, 17687−17691.
4. Bull, C., Niederhoffer, E. C., Yoshida, T., and Fee, J. A. (1991) Kinetic studies of superoxide dismutases: properties of the manganese-containing protein from *Thermus thermophilus*, *J. Am. Chem. Soc. 113*, 4069−4076.
5. Cabelli, D. E., Riley, D., Rodriguez, J. A. A., Valentine, J. S., and Zhu, H. (2000) Models of Superoxide Dismutases, in *Biomimetic Oxidations Catalyzed by Transition Metal Complexes* (Meunier, B., Ed.) Chapter 10, pp 461−508, Imperial College Press, London.
6. Hearn, A. S., Tu, C. K., Nick, H. S., and Silverman, D. N., (1999) Characterization of the product-inhibited complex in catalysis by human manganese superoxide dismutase, *J. Biol. Chem. 274*, 24457−24460.
7. Whittaker, M. M., and Whittaker, J. W. (1996) Low-temperature thermochromism marks a change in coordination for the metal ion in manganese superoxide dismutase, *Biochemistry 35*, 6762−6770.
8. Silverman, D. N., and Nick, H. S. (2002) Catalytic pathway of manganese superoxide dismutase by direct observation of superoxide, in *Methods in Enzymology*, Vol. 349, pp 61−74, Academic Press, New York.
9. Hsieh, Y., Guan, Y., Tu, C., Bratt, P. J., Angerhofer, A., Lepock, J. R., Hickey, M. J., Tainer, J. A., Nick, H. S., and Silverman, D.

N. (1998) Probing the active site of human manganese superoxide dismutase: the role of glutamine 143, *Biochemistry 37*, 4731−4739.
10. Guan, Y., Hickey, M. J., Borgstahl, G. E. O., Hallewell, R. A., Lepock, J. R., O'Connor, D., Hsieh, Y., Nick, H. S., Silverman, D. N., and Tainer, J. A. (1998) Crystal structure of Y34F mutant human mitochondrial manganese superoxide dismutase and the functional role of tyrosine 34, *Biochemistry 37*, 4722−4730.
11. Whittaker, M. M., and Whittaker, J. W. (1997) Mutagenesis of a proton linkage pathway in *Escherichia coli* manganese superoxide dismutase, *Biochemistry 36*, 8923−8931.
12. Beck, Y., Oren, R., Amit, B., Levanon, A., Gorecki, M., and Hartman, J. R. (1987) Human Mn superoxide dismutase cDNA sequence, *Nucleic Acids Res. 15*, 9076.
13. Carlioz, A., and Touati, D. (1986) Isolation of superoxide dismutase mutants in *Escherichia coli*: Is superoxide dismutase necessary for aerobic life? *EMBO J. 5*, 623−630.
14. Hearn, A. S., Stroupe, M. E., Cabelli, D. E., Lepock, J. R., Tainer, J. A., Nick, H. S., and Silverman, D. N. (2001) Kinetic analysis of product inhibition in human manganese superoxide dismutase, *Biochemistry 40*, 12051−12058.
15. Schwarz, H. A. (1981) Free radicals generated by radiolysis of aqueous solutions, *J. Chem. Educ. 58*, 101−105.
16. McRee, D. E., Redford, S. M., Getzoff, E. D., Lepock, J. R., Hallewell, R. A., and Tainer, J. A. (1990) Changes in crystallographic structure and thermostability of a Cu,Zn superoxide dismutase mutant resulting from the removal of a buried cysteine, *J. Biol. Chem. 265*, 14234−14241.
17. Lepock, J. R., Frey, H. E., and Hallewell, R. A. (1990) Contribution of conformational stability and reversibility of unfolding to the increased thermostability of human and bovine superoxide dismutase mutated at free cysteines, *J. Biol. Chem. 265*, 21612−21618.
18. Sturtevant, J. M. (1987) Biochemical Applications of Differential Scanning Calorimetry, *Annu. Rev. Phys. Chem. 265*, 463−488.
19. McClune, G. J., and Fee, J. A. (1978) A simple system for mixing miscible organic solvents with water in 10−20 ms for the study of superoxide chemistry by stopped-flow methods, *Biophys. J. 24*, 65−69.
20. Rabani, J., and Nielson, S. O. (1969) Absorption spectrum and decay kinetics of O_2^- and HO_2 in aqueous solutions by pulse radiolysis, *J. Phys. Chem. 73*, 3736−3744.
21. Otwinowski, Z., and Minor, W. (1997) Processing of X-ray Diffraction Data Collected in Oscillation Mode, in *Methods in Enzymology* (Carter, C. W., Jr., and Sweet, R. M., Eds.) Vol. 276, pp 307−326 Academic Press, New York.
22. Brunger, A. T., Adams, P. D., Clore, G. M., DeLano, W. L., Gros, P., Grosse-Kunstleve, R. W., Jiang, J. S., Kuszewski, J., Nilges, M., Pannu, N. S., Read, R. J., Rice, L. M., Simonson, T., and Warren, G. L. (1998) Crystallography & NMR system: A new software suite for macromolecular structure determination, *Acta Crystallogr. D54* (Part 5), 905−921.
23. McRee, D. E. (1999) XtalView/Xfit: A versatile program for manipulating atomic coordinates and electron density, *J. Struct. Biol. 125*, 156−165.
24. Adams, P. D., Pannu, N. S., Read, R. J., and Brunger, A. T. (1997) Cross-validated maximum likelihood enhances crystallographic simulated annealing refinement, *Proc. Natl. Acad. Sci. U.S.A. 94*, 5018−5023.
25. McAdam, M. E., Fox, R. A., Lavelle, F., and Fielden, E. M. (1977) A pulse-radiolysis study of the manganese-containing superoxide dismutase from *Bacillus stearothermophilus*: a kinetic model for the enzyme action, *Biochem. J. 165*, 71−79.
26. Miller, A.-F., Padmakumar, K., Sorkin, D. L., Karapetian, A., and Vance, C. K. (2003) Proton-coupled electron transfer in Fe-superoxide dismutase and Mn-superoxide dismutase, *J. Inorg. Biochem. 93*, 71−83.
27. Barshop, B. A., Wrenn, R. F., and Frieden, C. (1983) Analysis of numerical methods for computer simulation of kinetic processes: development of KINSIM-a flexible, portable system, *Anal. Biochem. 130*, 134−145.
28. Edwards, R. A., Whittaker, M. M., Whittaker, J. H., Baker, E. N., and Jameson, G. B. (2001) Outer sphere mutations perturb metal reactivity in manganese superoxide dismutase, *Biochemistry 40*, 15−27.
29. Maliekal, J., Karapetian, A., Vance, C., Yikilmaz, E., Wu, Q., Jackson, T., Brunold, T. C., Spiro, T. G., and Miller, A.-F. (2002) Comparison and contrasts between the active site p*K*s of Mn-superoxide dismutase and those of Fe-superoxide dismutase, *J. Am. Chem. Soc. 124*, 15064−15075.
30. Liang, Z., Xue, Y., Behravan, G., Jonsson, B. H., and Lindskog, S. (1993) Importance of the conserved active-site residues Tyr7, Glu106 and Thr199 for the catalytic function of human carbonic anhydrase II, *Eur. J. Biochem. 211*, 821−827.
31. Noodleman, L., Lovell, T., Han, W.-G., Li, J., and Himo, F. (2004) Quantum chemical studies of intermediates and reaction pathways in selected enzymes and catalytic synthetic systems, *Chem. Rev. 104*, 459−508.
32. Mildvan, A. S., Weber, D. J., and Kuliopulos, A. (1992) Quantitative interpretations of double mutations of enzymes, *Arch. Biochem. Biophys. 294*, 327−340.
33. Cabelli, D. E., Guan, Y., Leveque, V., Hearn, A. S., Tainer, J. A., Nick, H. S., and Silverman, D. N. (1999) Role of tryptophan 161 in catalysis by human manganese superoxide dismutase, *Biochemistry 38*, 11686−11692.
34. Davis, C. A., Hearn, A. S., Fletcher, B., Bickford, J., Garcia, J. E., Leveque, V., Melendez, J. A., Silverman, D. N., Zucali, J., Agarwal, A., and Nick, H. S. (2004) Potent anti-tumor effects of an active site mutant of human MnSOD: Evolutionary conservation of product inhibition, *J. Biol. Chem. 279*, 12769−12776.

BI049888K